A Few-shot Electromechanical Impedance Monitoring Method Based on a Modified Prototype Network

Fei Du[1,2], Shiwei Wu[1], Jiexin Weng[3], Xuan Zhang[3], Chao Xu[1,2] and Zhongqing Su[4,1]

[1]School of Astronautics, Northwestern Polytechnical University, Xi'an 710072, China
[2]Yangtze River Delta Research Institute of Northwestern Polytechnical University, Taicang 215400, China
[3]Inner Mongolia Power Machinery Research Institute, Hohhot 010000, China
[4]Department of Mechanical Engineering, The Hong Kong Polytechnic University, Kowloon, Hong Kong Special Administrative Region of China

E-mail: chao_xu@nwpu.edu.cn

Received xxxxxx
Accepted for publication xxxxxx
Published xxxxxx

Abstract

Bolt loosening monitoring is of great significance to warrant the reliability and safety of bolted structures. The electromechanical impedance (EMI)-based evaluation is effective to perceive bolt loosening. However, EMI signals are highly prone to contamination by temperature fluctuation. Deep learning (DL) based EMI is a promising technique for accurate damage detection in the temperature variation environment. However, DL needs a lot of data to train, which is usually very difficult to collect sufficient structural damage data in real word scenarios. This paper proposed a few-shot EMI monitoring method based on a modified prototype network for bolt looseness detection under temperature varying environment. The approach features a conversion method of the impedance signal to image based on the Hank matrix. A modified prototype network is then developed. An experimental study was carried out on a bolted joint. EMI signals under different bolt loosening conditions were measured in a temperature variation environment. An impedance analyzer and a self-made small lightweight monitoring device were both used to measure the EMI signals to test the cross domain scenario. The proposed method was compared with the transfer learning methods and other typical FSL methods. The experiment results show that the proposed few-shot EMI method can obviously improve the monitoring accuracy of bolt loosening with few samples.

Keywords: Bolt loosening, Few-shot learning, Modified prototype network, Electromechanical impedance, Temperature.

1. Introduction

Bolt joints are often used in engineering structures to connect different parts. However, bolts are frequently subjected to loosening due to inappropriate preloads during installation or time varying external loads during service[1]. Bolts loosening may lead to the failure of the entire structure. Hence, monitoring the preload states of bolt joints is of great significance to ensure the reliability and safety of the entire structure[2, 3]. Electromechanical impedance-based evaluation method (EMI) using active piezoelectric transducers is an effective technique for bolt loosening monitoring[4, 5]. By measuring the electrical impedance of a piezoelectric sensor attached to the monitored structure, the

change in the mechanical impedance of the structure can be evaluated[6, 7]. The EMI method is a local damage monitoring method and is sensitive to the initial loosening of a bolt. In the EMI damage detection, the real part of the measured impedance is perceptive to structural damage. The root mean square deviation (RMSD) or correlation coefficient (CC) of the real parts of impedance before and after the damage is often used as the damage index[4, 5].

In the practical engineering applications of the EMI method, the environment temperature of engineering structures changes continually. However, the change of temperature will directly lead to changes in the characteristics of the piezoelectric transducer and the adhesive layer, which greatly affect the accuracy of defect detection. Hence, the temperature compensation of the impedance spectrum must be considered. To this end, Koo et al[8] proposed an effective frequency shift method (EFS) to reduce the effect of temperature. This method shifts the real part curve of EMI on the frequency axis to maximize the CC index. However, it is hard to compensate for changes in EMI amplitude caused by temperature. Hence, Wandowski et al[9] further proposed to compensate for vertical shift of EMI by whole-signal normalization using root mean square (RMS) before the application of EFS. Although this method eliminated the influence of temperature better, the change in the shape of the EMI curve caused by temperature is still ignored, which also affects the detection accuracy.

To improve detection accuracy, the application of machine learning in EMI detection has been widely discussed by researchers. Park et al[10] calculated the RMSD of the principal components of EMI data extracted by principal component analysis (PCA). Then the k-means clustering network was used to cluster different numbers of loose bolts. Selva et al.[11] proposed to use Probabilistic Neural Networks(PNN) for the damage localization, and 7 damage indices including RMSD and CC were used as the input of the PNN. Recently, Na [12] used EMI technique with PNN to identify torque loss of bolts on three bolted structure specimens. To consider the effect of temperature, Min et al. [13] split the EMI signals into multiple sub-ranges of frequency, and calculated the temperature-compensated CC values for each sub-range by the EFS method[8]. Then the compensated CC values were used as inputs of a feedforward neural network (FNN) to classify damages. In the above machine learning techniques, damage indices need to be constructed artificially before using k-clustering, PNN or FNN.

In recent years, DL methods, especially convolutional neural networks (CNN), have been gradually used in structural health monitoring (SHM) [14, 15]. DL is a promising technique for accurate damage detection based on EMI, which does not need damage indices. Two-dimension (2-D) CNNs are commonly used in many domains, while EMI signals are one-dimension (1-D) frequency-domain signals. Hence, how to construct an image based on EMI signals is one of the key aspects. Choy et al. [16]used the frequency axis of the real part curve of EMI signal as the vertical axis, and extended its corresponding value in the horizontal direction. Thus, RGB images were constructed as the input of CNN. However, the image size is also the square of the signal length. De Oliveira et al. [17] split the real part of EMI signal into several parts and then computed the Euclidean distance among them to form an RGB image. A 2-D CNN with three convolution layers was established to identify the simulated damages on an aluminum board. However, it is complicated to calculate the Euclidean distance matrix. Almeida et al.[18] established a 1-D CNN and a 2-D CNN with only one convolutional layer in each model. For the 2-D CNN, EMI signal was divided into multiple segments, which were then directly stacked to construct an image as input, and 2,470 samples were used. However, this method will cause jumps at the cutoffs. The classification accuracy of the above two CNNs is not higher than 88.95%. The main reason is that only one convolutional layer cannot extract image features well.

The above works based on CNNs did not consider the influence of temperature. De Rezende et al.[19] established a 1-D CNN with only one convolutional layer to identify simulated damages on aluminum plates, and 900 samples were used. However, only three different temperatures were considered. Du et al.[20] proposed a multi-task U-Net CNN to carry out temperature compensation and bolt loosening condition monitoring of bolted structures based on EMI signals. It is proved that the DL based EMI damage monitoring method is effective and accurate in the temperature variation environment.

DL needs a lot of data to train. However, it is usually very difficult to collect sufficient structural damage data in real word scenarios[21]. The problem of training a DL network with few labeled samples (e.g., one or five samples per class) during network training is known as few-shot learning (FSL) [22]. It has received very much attention in recent years. An FSL task usually contains an auxiliary set, a target labeled support set and a target unlabeled query set. Unlike transfer learning, FSL methods usually employ an episodic training mechanism[23] to train the network. This is done by sampling a large number of episodes from the auxiliary training set, each of which is a simulation of the test task. In this way, the trained model can converge quickly on the test task[24].

Typical FSL methods can be roughly divided into two types: meta-learning based methods and metric-learning based methods[22]. The metric-learning based methods adopt the learning-to compare paradigm to classify query samples by comparing the distance between query samples and support samples. It has received a lot of attention. Vinyals et al. [23] proposed a MatchingNet, which uses LSTM as the embedding function and cosine similarity to measure the distance between

query samples and labeled samples. Sung et al.[25] developed a RelationNet using an embedded module consisting of four layers of CNN to extract features, and a relationship module consisting of two layers of CNN for distance measurement. Over fitting is the key problem of FSL. To solve this problem, Snell et al.[26] proposed a ProtoNet, which compares the Euclidean distance between query samples and prototypes of each class in an embedded space for few-shot classification. ProtoNet has a very simple model architecture. However, the metric function of the ProtoNet needs to be further improved to increase the generalization ability of the model.

Recently, FSL method has been gradually applied to fault diagnosis and SHM. Wu et al.[27] verified the performance of the RelationNet in fault diagnosis on three bearing fault datasets. The results show that the RelationNet is effective in extremely few-shot classifications. Tao et al. [28] proposed a model unknown matching network for fault diagnosis problem by combining a meta-learning network and a metric-learning network. In the field of image-processing based SHM, Xu et al.[29] proposed a nested attribute-based few-shot meta learning paradigm for structural damage identification. It can be seen that FSL has achieved good performances in few-shot fault diagnosis and image-based SHM. However, it has not been applied in EMI-based SHM.

In this paper, a few-shot EMI monitoring method based on a modified prototype network is proposed for bolt looseness detection under temperature varying environment. The contributions of this paper are as follows.

(1) A few-shot EMI monitoring method based on a modified prototype network for damage detection is proposed. First, the Hank matrix is used to convert the 1-D EMI signal into a 2-D image. Then, the metric function of the prototype network is improved by adopting the cosine similarity to calculate the distance between the sample and the prototype.

(2) Datasets simulating the real service environment were constructed to validate the proposed method. The EMI signals under different bolt loosening conditions were measured in a temperature change environment. In addition, an impedance analyzer and a self-made small lightweight monitoring device were both used to measure the EMI signals to test the cross domain scenario.

(3) Comparison analysis among the proposed method, the traditional EMI monitoring method based on damage index, transfer learning methods and other typical FSL methods is performed.

2. EMI Monitoring: Principle and Theory

PZT sensors can realize the mutual conversion of electrical and mechanical energy. For the EMI detection method, a PZT is usually glued to the base structure, as shown in Figure 1a. The length, width and height of the PZT are l_a, b_a and t_a, respectively. At this time, the PZT is constrained by the structural stiffness of the base structure k_{str}. The structural stiffness can be split into two end components[30], as shown in Figure 1b.

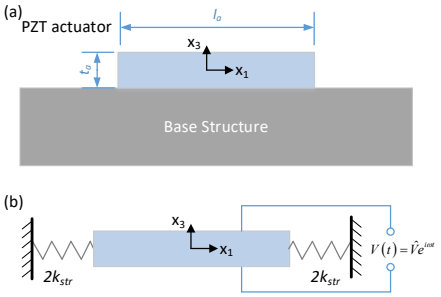

Figure 1. Structure with PZT pasted on it (1) Schematic diagram of the actual structure (b)Simplified boundary conditions

According to the above boundary conditions, constitutive equation of PZT, and axial waves equation, the electrical impedance of the PZT under excitation of harmonic voltage can be expressed by the following formula[4, 30]

$$\mathrm{Z} = \frac{1}{i\omega C}\left[1 - k_{31}^2\left(1 - \frac{1}{r+\varphi\cot\varphi}\right)\right]^{-1} \quad (1)$$

where, ω is the angular frequency, C is the capacitance of the PZT, k_{31}^2 is the electromechanical coupling factor, $\mathrm{r} = k_{str}/k_{PZT}$ is the stiffness ratio of the PZT sheet and the base structure. φ can be expressed as

$$\varphi = \frac{1}{2}\gamma l_a \quad (2)$$

where, γ is the wave number. When the PZT is used in a frequency sweep, the structural stiffness, k_{str} will vary with frequency, going through zero at structural resonances, and extreme values at structural anti-resonances[30]. At this time, the electrical impedance Z changes significantly. Thereby, damages caused by the change of k_{str} can be evaluated.

In practice, the most popular damage indices used in the EMI method are the root mean square deviation (RMSD) and the correlation coefficient(CC), which can be written as[31, 32]:

$$\mathrm{RMSD} = \sum_{\omega_I}^{\omega_F}\sqrt{\frac{\left[Re(Z_2(\omega)) - Re(Z_1(\omega))\right]^2}{Re(Z_1(\omega))^2}} \quad (3)$$

$$\mathrm{CC} = \frac{cov\left[Re(Z_1(\omega)), Re(Z_2(\omega))\right]}{\sigma_1\sigma_2} \quad (4)$$

where, $\mathrm{Re}(Z_1(\omega))$ is the real part of the baseline signal, $\mathrm{Re}(Z_2(\omega))$ is the real part of the impedance signal after possible damage, ω_I and ω_F are the initial frequency and final frequency, cov is the covariance of the two impedance signals, σ_1 and σ_2 are the corresponding standard deviations of each signal.

In fact, the properties of PZT, such as capacitance, change with temperature. Therefore, as the temperature increases, the real part of the impedance shifts to the low frequency direction of the frequency axis[9]. At the same time, its amplitude decreases and the shape of the impedance curve changes slightly. If temperature compensation is not performed, the damage index obtained by Eqs. (3) or (4) will result in a false warning [33].

3. The few-shot EMI monitoring method

This section presents a few-shot EMI monitoring method based on a modified prototype network. A 1-D EMI signal is transformed into a 2-D image using a Hank matrix as the input to the network.

3.1 The episodic training mechanism

In few-shot setting, there are usually three sets of data, i.e. a target labeled support set $\mathcal{S}$, a target unlabeled query set $\mathcal{Q}$ and a class-disjoint auxiliary set $\mathcal{A}$. In addition, $\mathcal{S}$ and $\mathcal{Q}$ share the same label space. If the support set contains C classes with K labelled samples, the classification task is called a C-way K-shot task[22, 25]. To learn an effective FSL classifier, episodic training mechanism[23] is normally adopted at the training stage. Episodic-training relies on lots of simulation few-shot tasks, which are randomly constructed from the auxiliary set $\mathcal{A}$. Each simulated task (episode) $\mathcal{T}$ consists of two subsets, $\mathcal{A}_{\mathcal{S}}$ and $\mathcal{A}_{\mathcal{Q}}$, which are akin to $\mathcal{S}$ and $\mathcal{Q}$, respectively. In one training epoch, lots of episodes will be randomly sampled from the auxiliary set to train this model[22], as shown in

$$\left\{\mathcal{T}^i = \langle \mathcal{A}_{\mathcal{S}}^i, \mathcal{A}_{\mathcal{Q}}^i \rangle\right\}_{i=1}^{N} \tag{5}$$

where N is the number of episodes.

3.2 The modified prototype network based on the cosine similarity

The Prototype network is a typical metric-learning based FSL method. The metric-learning methods usually consist of two modules, an embedding module and a metric module. The embedding module embeds each sample to a lower-dimensional representation space, and the metric module directly compares the distances between the query samples and support classes. Then, their distances are used to classify[34]. The Prototype network is based on the idea that there exists an embedding in which points cluster around a single prototype representation for each class.

The Prototype network computes an M-dimensional representation vector of a sample through an embedding function $f_\theta(\cdot)$ which is usually a CNN. The mean representation vector of the support samples in each class is taken as the prototype belonging to this class. Specifically, given a few-shot task $\mathrm{T} = \{\mathcal{S}, \mathcal{Q}\}$, the prototype of each class can be formulated as [26],

$$\mathbf{c}_\mathrm{i} = \frac{1}{K}\sum_{k=1}^{K} \mathbf{z}_\mathrm{k} = \frac{1}{K}\sum_{k=1}^{K} f_\theta(\mathbf{x}_\mathrm{k}) \tag{6}$$

where $\mathbf{x}_\mathrm{k}$ is the input feature, $\mathbf{z}_\mathrm{k}$ is the embedding vector and K is the number of samples in each class (K-shot).

Different from the Prototype network, the modified Prototype network uses cosine distance instead of Euclidean distance to compare the similarity between query samples and each prototype for classification. The cosine distance can be written as,

$$d_{cos}(\mathbf{z}_j, \boldsymbol{c}_i) = 1 - \cos(\mathbf{z}_j, \boldsymbol{c}_i) = 1 - \frac{\mathbf{z}_j \cdot \boldsymbol{c}_i}{\|\mathbf{z}_j\| \|\boldsymbol{c}_i\|} \tag{7}$$

where $\mathbf{z}_\mathrm{j}$ is the embedding vector of query sample j.

Finally, the posterior probability of query sample j belonging to class i is calculated using the softmax function, as shown below.

$$p(y = i|Q) = \frac{exp\left(-d_{cos}(\mathbf{z}_j, \boldsymbol{c}_i)\right)}{\sum_{u=1}^{C} exp\left(-d_{cos}(\mathbf{z}_j, \boldsymbol{c}_u)\right)} \tag{8}$$

The structure of the improved prototype network is shown in Fig. 2.

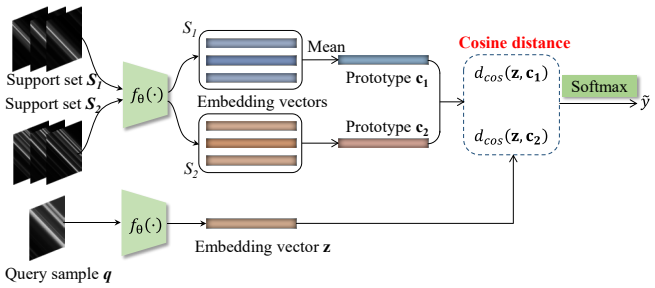

Figure 2. The structure of the modified Prototype network

The embedding function in the modified Prototype Network is composed of four convolutional blocks[35]. Each block comprises a 64-filter 3×3 convolution, batch normalization layer, a ReLU nonlinearity and a 2×2 max-pooling layer. The length of the embedded vector is 1600.

3.3 Input feature based on Hankel matrix

Impedance signal is a 1-D frequency domain signal. A Hankel matrix is a square matrix in which each ascending skew-diagonal from left to right is constant, as shown below:

$$A = \begin{bmatrix} a_0 & a_1 & \cdots & a_{n-1} \\ a_1 & a_2 & \cdots & a_n \\ \vdots & \vdots & & \vdots \\ a_{n-1} & a_n & \cdots & a_{2n-2} \end{bmatrix} \quad (9)$$

The Hankel matrix formed from the signal has been found useful for decomposition of non-stationary signals and time-frequency representation[36]. Besides, the adjacent pixels in the obtained image are continuous. Therefore, the Hank matrix is used to convert the EMI signals into an image.

Data normalization can improve training efficiency and network generalization performance. Therefore, each real part of impedance signal is normalized using the Min-Max Normalization method before converting to Hank matrix, as shown below:

$$\mathrm{Re}\left(\hat{Z}(\omega)\right) = \frac{Re(Z(\omega)) - \min\left(Re(Z(\omega))\right)}{\max\left(Re(Z(\omega))\right) - \min\left(Re(Z(\omega))\right)} \quad (10)$$

Then, $\mathrm{Re}\left(\hat{Z}(\omega)\right)$ is converted to Hank matrix. The matrix is finally transformed into an 8-bit grayscale image, which is used as the input of the improved Prototype Network. The size of the grayscale image used in this study is 224×224 pixels.

4. Experimental Validation

Experimental validation was carried out on a lap joint connected by two bolts. EMI signals were measured from PZT pasted on the joint to verify the proposed method and its adaptability to cross domain scenarios.

4.1 Experimental specimen and apparatus

The experimental specimen is a bolted lap joint, as shown in Figure 3. The bolts are steel M6 bolts of strength grade 8.8, which connect two aluminum plates together. The thickness of each aluminum plate is 3mm. Flat washers were used for each bolt. A PZT sensor of P5-H was pasted between the two M6 bolts with AB glue. The dimensions of the PZT sensor are 10mm×8mm×0.5mm.

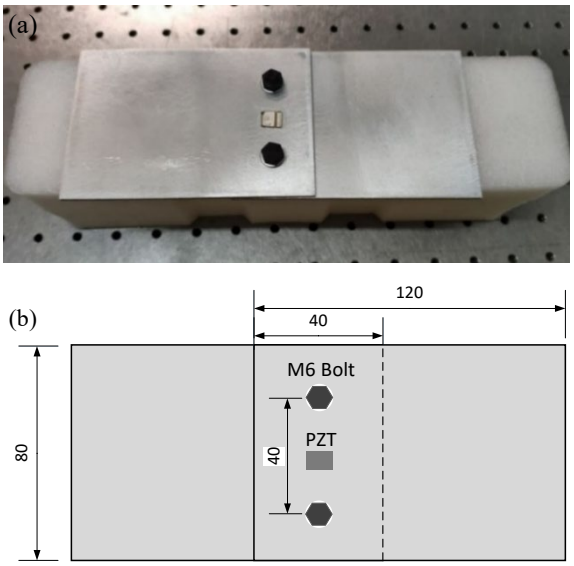

Figure 3. The bolted lap joint (a) Photo of the bolted lap joint, (b) Dimensions of the specimen (Unit: mm)

In the experiment, a digital torque wrench of STANLEY SD-030-22 was used to tighten the two M6 bolts. An isothermal box 202-00A was used to change and maintain the temperature of the specimen, as shown in Fig. 4. The temperature in the box was accurately monitored through a four-wire thermistor PT100. The EMI measurement was performed when the monitored temperature in the box was stable.

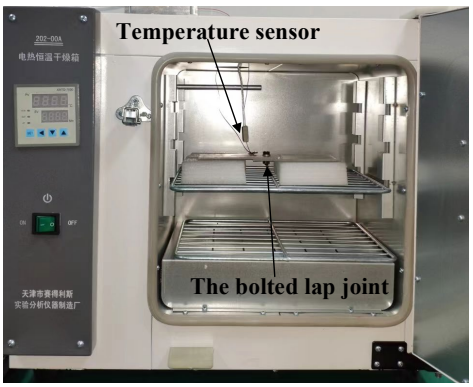

Figure 4. The impedance measurement in the isothermal box.

An impedance analyzer of HIOKI IM3570 was used to measure the impedance signals from the PZT. SHM relies on small lightweight instruments. Hence, a self-made EMI monitoring device[37] based on AD5933 chip was also used to measure the EMI signals to test the cross domain scenario. When the temperature was 25℃ and the torque of the two M6 bolts was 10N·m (health status of bolted joints), the specimen was pre-swept by the impedance analyzer HIOKI IM3570. The frequency sweep range is from 10kHz to100kHz, and the real part of the measured impedance is shown in Figure 5.

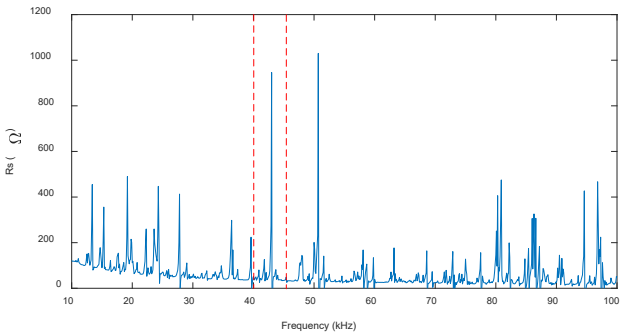

Figure 5. Real part of the pre-swept impedance

It can be seen that there are multiple resonance peaks in the range from 10 to 100kHz. The resonance peak amplitude is relatively large from 40 kHz to 55kHz. To reduce the data length, the measurement frequency range of 40kHz~45kHz is selected in the following measurement, as shown by the dotted line in Figure 5.

4.2 Damage scenarios and datasets

Nine damage scenarios were measured by the impedance analyzer, as listed in Table 1 (1-1 represents the torque of both bolts 1N·m). There are a total of 720 sets of data. For each damage scenario, the bolts were tightened 3 times by the torque wrench. Therefore, three tightening batches were performed for all the damage scenarios. It should be noted that the temperature is evenly distributed within the temperature range for each damage scenario.

Table 1. Damage scenarios measured by the impedance analyzer

Damage scenario	Torques of the two bolts(N·m)	Temperature range(℃)	Device	Number of signals
1	1-1	16~70	IM3570	80
2	1-4	16~70	IM3570	80
3	1-8	16~70	IM3570	80
4	4-1	16~70	IM3570	80
5	4-4	16~70	IM3570	80
6	4-8	16~70	IM3570	80
7	8-1	16~70	IM3570	80
8	8-4	16~70	IM3570	80
9	8-8	16~70	IM3570	80

The self-made EMI monitoring device was used to measure four damage scenarios, as listed in Table 2. In this measurement, the bolts were tightened once for every damage scenario. Before the measurement, the AD5933 chip was calibrated by a resistance of 3000Ω. It can be seen that damage scenarios 10, 11, 12, and 13 are close to damage scenarios 1, 3, 7, and 9 in Table 2, respectively.

Table 2. Damage scenarios measured by the self-made monitoring device

Damage scenario	Torques of the two bolts(N·m)	Temperature range(℃)	Device	Number of signals
10	0-0	24~60	AD5933	107
11	0-10	24~60	AD5933	99
12	10-0	24~60	AD5933	98
13	10-10	24~60	AD5933	102

In the training phase, a total of 720 samples from damage scenarios 1-9 formed an auxiliary set on which episode training was performed. Among them, categories 1, 3, 5, 7 and 9 were used as the auxiliary training set, and the remaining 4 categories were used as the auxiliary validation set. In the testing phase, a total of 406 samples from categories 10-13 listed in Table 2 were used as the test set. For the auxiliary set, the temperature distribution is shown in Fig. 6a. For the test set, the temperature distribution is shown in Fig. 6b.

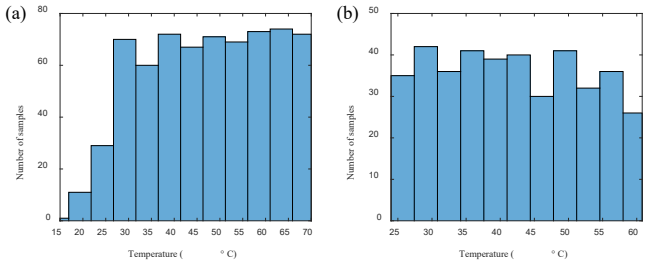

Figure 6. The temperature distributions (a) the auxiliary set (b) the test set

4.3 EMI signals under different temperatures

Figure 7 shows the real part of EMI signals of damage scenarios 1, 3, 7, and 9. Three signals are selected from each damage scenario, and the corresponding temperatures are around 24, 40, and 60℃. Figure 7a and d show that as the temperature increases, the resonance peak of the impedance shifts to the low-frequency direction, and the amplitude changes slightly. Meanwhile, the shapes of the curves in Figure 7b and c change greatly. The reason is that the signals in each subplot were measured in three different tightening batches. In addition, Figure 7b and c show that the impedance curves of damage scenarios 3 and 7 under the same temperature are different. The main reason is that the structure is not symmetrical due to the dimensional deviations and the preload deviations

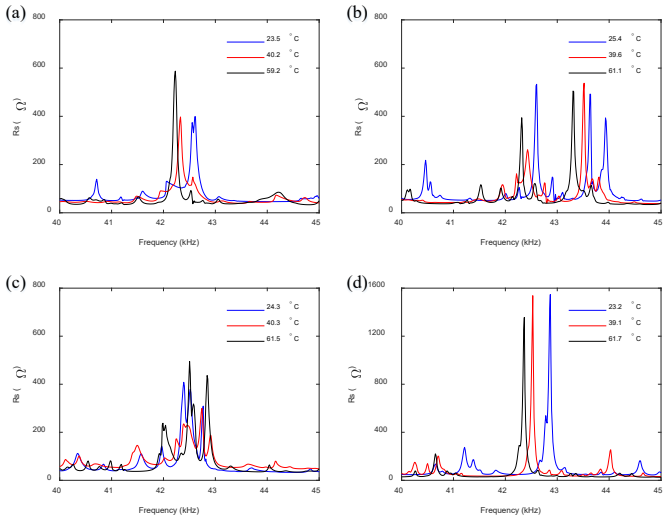

Figure 7. The real parts of measured impedances (a) Damage scenario 1, (b) Damage scenario 3, (c) Damage scenario 7, (d) Damage scenario 9.

Figure 8 shows the real part of the EMI signals of damage scenarios 10-13. Each subplot also shows 3 curves from the same damage scenario, and the corresponding temperatures are around 24, 40, and 60 ℃. It is obvious that as the temperature increases, the resonance peak shifts to the low frequency direction, and the corresponding amplitude decreases. Compared with Figure 7, it can be seen that all the curves displayed in Figure 8 shift upward. The impedance amplitudes measured by the AD5933 are different from the impedance analyzer measurements. This difference is due to the characteristics of the chip AD5933[10]. Thus the auxiliary set and the support and query sets are cross-domain scenarios, which leads to difficulties for few-shot classification.

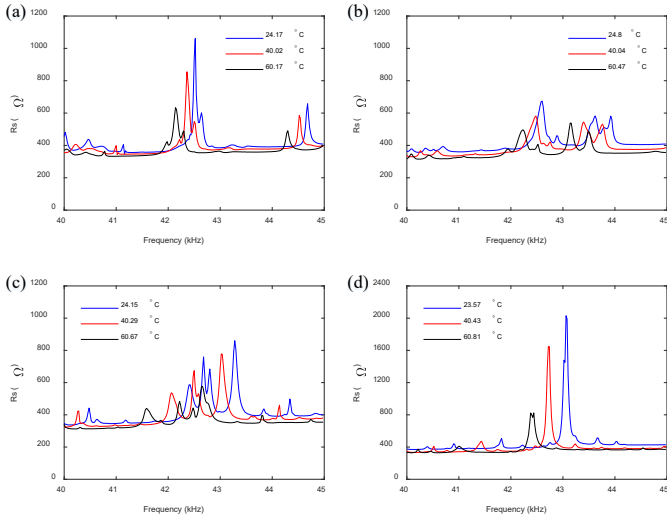

Figure 8. The real parts of measured impedances (a) Damage scenario 10, (b) Damage scenario 11, (c) Damage scenario 12, (d) Damage scenario 13.

5 . Results and discussion

The modified prototype network was used to identify the damage scenarios measured by the experiment in Section 4. The results were compared with the traditional EMI monitoring method based on damage index, the transfer learning methods and other typical FSL methods.

5.1 Training process and hyperparameters

The measured impedance signals were converted into 224×224 pixel grayscale images using the method in Section 4.3. Fig.9 shows the grayscale images converted from the impedance curves measured at around 24°C shown in Figs. 7 and 8. It can be seen that the white stripes in each image change with the damage scenario. Furthermore, the white stripes shift in their vertical direction with temperature.

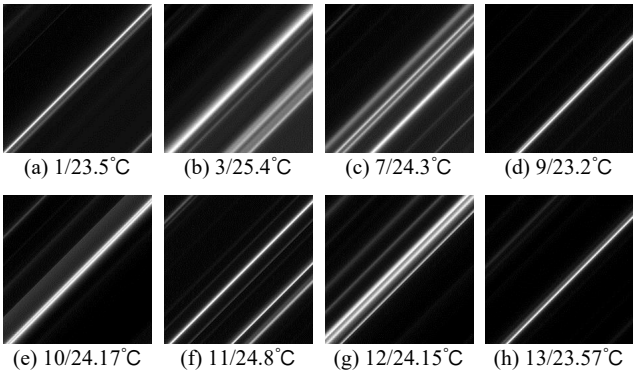

Figure 9. The input grayscale images

In this paper, 4-way 4-shot and 4-way 1-shot tasks were investigated. 4-way 4-shot task means the support set contains 4 classes with 4 labelled samples. 4-way 1-shot task means the support set contains 4 classes with 1 labelled sample. At this time, the episode training process is as follows. First, 4 categories were randomly sampled from the auxiliary training set. And each category in one episode contains 4 or 1 support samples and 15 query samples, which were randomly selected from the total number of 80 samples in each category. In this way, 15 episodes were generated from the auxiliary training set. Using the same procedure, the same number of episodes were generated from the auxiliary validation set. In each epoch, the episodes from the auxiliary training set were used to train the embedding function, and the model was evaluated on the episodes from the auxiliary validation set. The model was saved when the validation accuracy is highest.

Then, the 4-way 4-shot and 4-way 1-shot tasks were tested to evaluate the performance of the saved model. In each episode, 4 or 1 support sample and 15 query samples were randomly selected from each of categories 10-13. Each task was tested with 50 episodes, and the mean and variance of classification accuracy were finally calculated.

During network training, the Adam optimization method[38] was used to optimize the network parameters. The learning rate has a great effect on the training process, so it was optimized. For the two tasks, the learning rate are 8e-3 and 2e-3, respectively.

5.2 Results of damage index after temperature compensation

The results shown in Figs.7 and 8 were compensated by the method of Wandowski et al. [9]. The impedance curves shown in Fig. 7 after temperature compensation are displayed in Fig. 10. It can be seen that the effect of temperature cannot be completely eliminated. Then, the RMSD and CC were calculated by Eq.3 and 4, and are displayed in Fig. 11. In this figure, the first curve means the result of the blue curve in Fig. 7, the second curve means that of the red curve and the third curve means that of the black curve. For damage scenarios 1, 3, 7 and 9, the curve in damage scenario 9 measured at 23.2℃ was used as the baseline signal. For damage scenarios 10-13, the curve in damage scenario 13 measured at 23.57°C was used as the baseline signal.

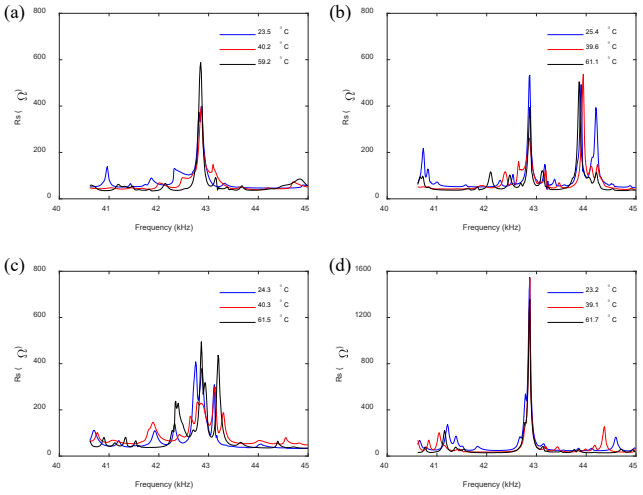

Figure 10. The real parts of measured impedances after temperature compensation (a) Damage scenario 1, (b) Damage scenario 3, (c) Damage scenario 7, (d) Damage scenario 9.

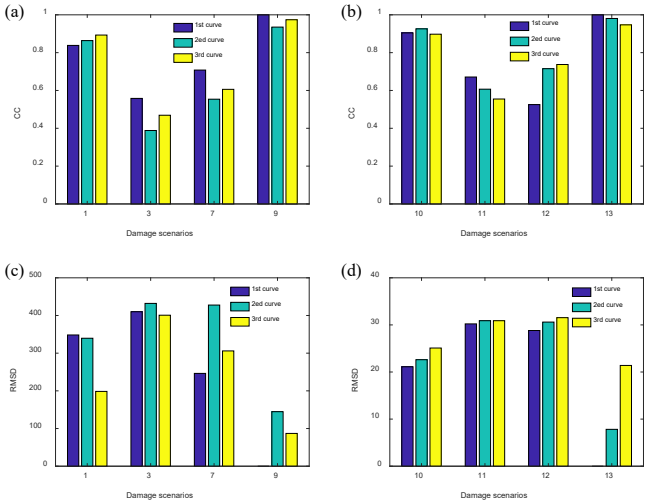

Figure 11. Damage indices after temperature compensation (a) CC indices of damage scenarios 1, 3, 7, 9, (b) CC indices of damage scenarios 10-13, (c) RMSD indices of damage scenarios 1, 3, 7, 9, (d) RMSD indices of damage scenarios 10-13.

It can be seen from Fig. 11a that after temperature compensation, damage scenarios 1 or 9 can be identified from others by using the CC index. However, the CC indices of damage scenarios 3 and 7 are too close and cannot be distinguished. It should be noted that the CC value of the baseline is 1. Similarly, the results in Fig. 11b show that damage scenarios 11 and 12 cannot be distinguished from each other after temperature compensation. Figure 11c also shows that damage scenarios 1, 3 and 7 cannot be distinguished from each other by RMSD values after temperature compensation. It should be noted that the RMSD value of the baseline signal is 0. Similarly, damage scenarios 11 and 12 cannot be distinguished from each other by RMSD as shown in Figure 11d. It can be concluded that it is difficult to accurately identify every damage scenario by traditional methods based on temperature compensation and damage indices. Hence, the temperature compensation method is not used in the proposed FSL method.

5.3 Results of the proposed method

The proposed method is verified, and the training procedure in Section 5.1 is used. The classification accuracy in the test set is compared with the results of typical FSL methods, including the ProtoNet, RelationNet, MatchingNet, and MAML. Note that the same four-layer convolution backbone is used in the above method, and the hyperparameters are the same. The 4-way 4-shot and 4-way 1-shot tasks were tested respectively. The mean and standard deviation of the results are listed in Table 3.

At the same time, the proposed method was compared with the transfer learning methods based on network fine-tuning, including the Baseline and Baseline++[35]. Both the Baseline

and the Baseline++ methods use the same four-layer convolution backbone. Their classifiers are the softmax classifier and the cosine distances based classifier[35], respectively. The Baseline and Baseline++ models were pre-trained using the entire auxiliary training set. Then, the classifiers of the models were fine-tuned by the support set of an episode in the test set. And the query set of the same episode is used to verify the classification accuracy. When the classifier was fine-tuned, the parameters of the convolution layers were fixed. 50 episodes of data in the test set were randomly selected, and the above fine-tuning procedures were repeated 50 times. The mean and variance of classification accuracies were finally calculated, and the results were listed in Table 3.

Table 3. Classification accuracy of the FSL and transfer learning methods

Method	Accuracy (%)	
	4-way 4-shot	4-way 1-shot
Baseline	94.03 ± 1.57	85.53 ± 2.57
Baseline++	91.20 ± 1.03	86.90 ± 1.27
RelationNet	94.33 ± 0.82	91.30 ± 1.93
MatchingNet	97.07 ± 0.85	89.70 ± 1.51
MAML	93.30 ± 1.18	89.20 ± 1.43
ProtoNet	93.67 ± 0.92	88.53 ± 1.98
Modified ProtoNet	**97.63 ± 0.48**	**93.43 ± 0.92**

It can be seen from the results in Table 3 that, the proposed modified Prototype Network has the highest precision and smallest standard deviation on the test set. The accuracy improvement of the modified Prototype Network is obvious for both the 4-way 4-shot and 4-way 1-shot tasks, especially for the 4-way 1-shot task. The effectiveness of the proposed method has been verified. In addition, the results also show that the accuracies of all the FSL methods are higher than those of the transfer learning methods for the 4-way 1-shot task. It indicates that the episodic training mechanism is more effective than the fine-tune based transfer learning method in extremely few-shot classifications. Figure 12a and b show the confusion matrices of two episodes in the 4-way 1-shot task and the 4-way 4-shot task, respectively.

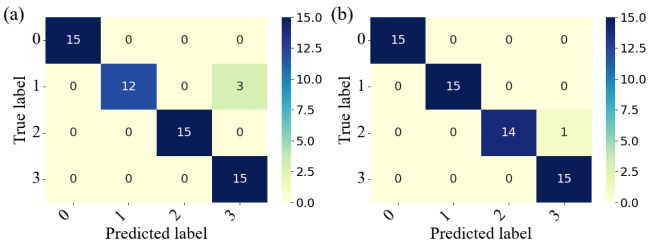

Figure 12. The confusion matrices of the classification results for the modified ProtoNet (a) the 4-way 1-shot task, (b) the 4-way 4-shot task.

For the proposed method, the classification accuracies under different embedded vector lengths were compared, and the results are listed in Table 4:

Table 4. Classification accuracy with different embedded vector lengths

Embedded vector length	Accuracy (%)	
	4-way 4-shot	4-way 1-shot
1600	**97.63 ± 0.48**	93.43 ± 0.92
1400	96.40±0.93	91.70± 1.85
1200	96.27±0.85	91.43± 2.25
800	95.57±0.72	**95.13± 1.45**
400	95.20±0.71	92.53± 1.26
200	93.50±1.09	84.53±2.05

It can be seen that the length of the embedded vector has a greater impact on the test accuracy. For the 4-way 4-shot task, the classification accuracy is the highest when the embedded vector length is 1600. For the 4-way 1-shot task, the classification accuracy is the highest when the length is 800. The size of the input image is 224 × 224. When the embedded vector is too short, such as 400 or 200, it is difficult for the embedded vector to represent the overall characteristics of the sample. At this time, its classification accuracy is poor.

For the 4-way 4-shot task, the classification accuracy increases with the vector length. The reason is that there are multiple support samples in one class of the support set, and the prototype calculated from the support samples can better represent the overall characteristics of the class. The feature information is richer when the prototype length is larger. However, for the 4-way 1-shot task, there is only one support sample in one class of the support set, and its embedded vector is used as the prototype of the entire class. If the prototype length is too large, it will contain too many details of the sample itself. These details cannot accurately represent the overall characteristics of the class, which have a negative impact on the classification. Therefore, the classification accuracy of the 4-way 1-shot task does not always increase with the length of the embedded vector.

5.4 The effect of the cosine distance

To show the advantage of the cosine distance, the embedding vectors obtained by the ProtoNet and the modified ProtoNet were compared. The embedding vectors were visualized using the t-distributed stochastic neighbor embedding (t-SNE). In addition, the distribution discrepancy between the embedding vectors from different datasets was measured using the maximum mean discrepancy(MMD).

The t-SNE results of the embedding vectors from the auxiliary validation set and the test set are shown in Figs. 13 and 14. The embedding functions of the 4-way 1-shot and 4-way 4-shot tasks were used for Figs. 13 and 14, respectively.

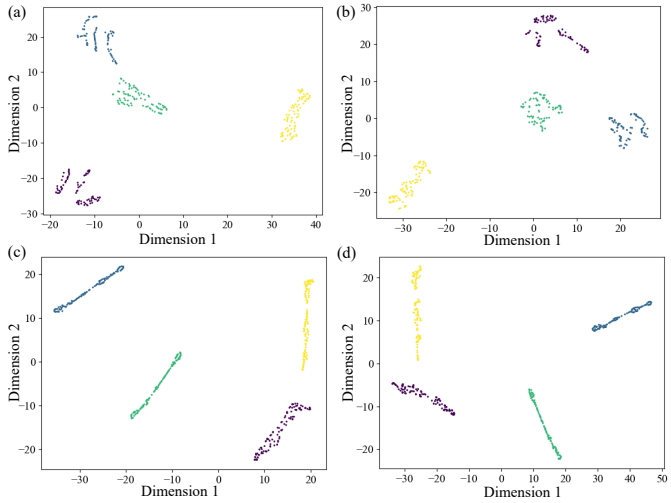

Figure 13. The t-SNE results of the embedding vectors for the 4-way 1-shot task calculated by (a) the ProtoNet from the auxiliary validation set, (b) the modified ProtoNet from the auxiliary validation set, (c) the ProtoNet from the test set, (d) the modified ProtoNet from the test set.

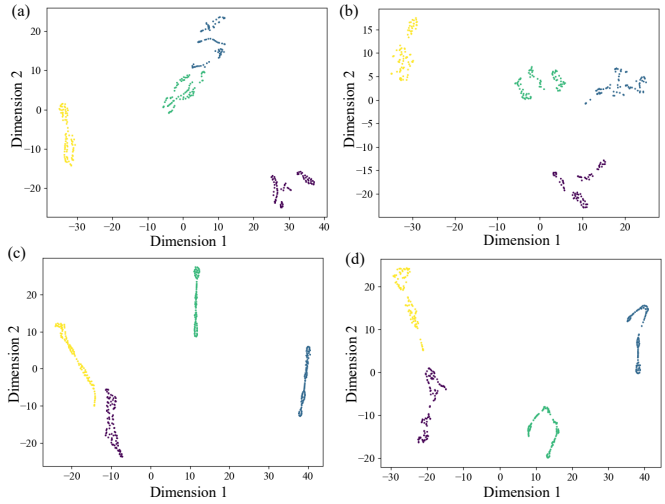

Figure 14. The t-SNE results of the embedding vectors for the 4-way 4-shot task calculated by (a) the ProtoNet from the auxiliary validation set, (b) the modified ProtoNet from the auxiliary validation set, (c) the ProtoNet from the test set, (d) the modified ProtoNet from the test set.

Figure 13a and b clearly show that the cosine distance can effectively increase the inter-class distances of embedding vectors from the auxiliary validation set. The results in Fig. 14 a and b are consistent with these in Fig. 13a and b. For the test set, Fig. 13c and d proved that the cosine distance can increase the inter-class distances of embedding vectors. The results in Fig. 14c and d are consistent with these in Fig. 13c and d.

Maximum mean discrepancy is a nonparametric distance metric that can measure the distribution discrepancy between two datasets. The MMD results between the embedding vectors calculated from the auxiliary and the test sets are listed in Table 5. The embedding vectors are calculated by the ProtoNet and the modified ProtoNet, respectively. It should be noted that the impedances in the test set were measured by the self-made EMI monitoring device. Moreover, the impedances in the auxiliary set were measured by the impedance analyzer of HIOKI IM3570. Table 5 shows that the distribution discrepancy can be reduced by the modified ProtoNet. This is better for the cross-domain classification.

Table 5. The MMD results

	ProtoNet	Modified ProtoNet
4-way 1-shot	0.7689	0.6380
4-way 4-shot	0.7357	0.4954

6 . Conclusion

This paper proposed a few-shot EMI monitoring method based on a modified prototype network for bolt looseness detection under temperature varying environment. In this method, impedance signals are converted into images by the Hankel matrix. A modified prototype network is developed by adopting the cosine similarity as the metric function. An experimental study was carried out on a lap joint connected by two bolts to construct realistic datasets. The EMI signals under different bolt loose conditions were measured under temperatures, varying from 16℃ to 70℃. An impedance analyzer and a self-made small lightweight monitoring device based on AD5933 were both used to measure the EMI signals to test the cross domain scenario. Comparison analysis among the proposed method, the traditional EMI monitoring method based on damage index, the transfer learning methods and other typical FSL methods is performed.

The experiment results show that the proposed method outperforms the other methods. The accuracy improvement of the modified Prototype Network is obvious for both the 4-way 4-shot and 4-way 1-shot tasks, especially for the 4-way 1-shot task. It is proved that the cosine distance can effectively increase the inter-class distances of embedding vectors and reduce distribution discrepancy of different domains. This is better for the cross-domain classification. The length of the embedded vector has a greater impact on the test accuracy. In addition, the results also show that the accuracies of all the FSL methods are higher than those of the transfer learning methods for the 4-way 1-shot task. It indicates that the episodic training mechanism is more effective than the fine-tune based transfer learning method in extremely few-shot

classification. Moreover, it is difficult to accurately identify every damage scenario by traditional methods based on temperature compensation and damage indices.

In summary, the proposed few-shot EMI method can provide accurate monitoring of bolt loosening with few samples and good generalization performance. Therefore, it has the potential to be applied to actual engineering structures in the service environment.

7. Funding

This study is supported by the National Natural Science Foundation of China (Grant No. 52075445). This study is also supported by Key Research and Development Program of Shaanxi (Program No.2021ZDLGY11-10)

References

[1] Wang F. Identification of multi-bolt head corrosion using linear and nonlinear shapelet-based acousto-ultrasonic methods. *Smart Materials and Structures*. 2021;**30**(8).

[2] Zhang X, Yan Q, Yang J, Zhao J, Shen Y. An assembly tightness detection method for bolt-jointed rotor with wavelet energy entropy. *Measurement*. 2019;**136**:212-24.

[3] Chen D, Huo L, Song G. High resolution bolt pre-load looseness monitoring using coda wave interferometry. *Structural Health Monitoring*. 2021;**21**(5):1959-72.

[4] Giurgiutiu V. *Structural Health Monitoring with Piezoelectric Wafer Active Sensors* 2ed. 225 Wyman Street, Waltham, MA 02451, USA: Elsevier; 2014. 1024 p.

[5] CR F, K W. *Structural health monitoring: a machine learning perspective*. Chichester: John Wiley & Sons; 2013. 161-243 p.

[6] de Castro BA, Baptista FG, Ciampa F. New imaging algorithm for material damage localisation based on impedance measurements under noise influence. *Measurement*. 2020;**163**.

[7] Du F, Wang G, Weng J, Fan H, Xu C. High-Precision Probabilistic Imaging for Interface Debonding Monitoring Based on Electromechanical Impedance. *AIAA Journal*. 2022:1-11.

[8] Koo K-Y, Park S, Lee J-J, Yun C-B. Automated Impedance-based Structural Health Monitoring Incorporating Effective Frequency Shift for Compensating Temperature Effects. *Journal of Intelligent Material Systems and Structures*. 2009;**20**(4):367-77.

[9] Wandowski T, Malinowski PH, Ostachowicz WM. Temperature and damage influence on electromechanical impedance method used for carbon fibre–reinforced polymer panels. *Journal of Intelligent Material Systems and Structures*. 2017;**28**(6):782-98.

[10] Park S, Lee J-J, Yun C-B, Inman DJ. Electro-Mechanical Impedance-Based Wireless Structural Health Monitoring Using PCA-Data Compression and k-means Clustering Algorithms. *Journal of Intelligent Material Systems and Structures*. 2007;**19**(4):509-20.

[11] Selva P, Cherrier O, Budinger V, Lachaud F, Morlier J. Smart monitoring of aeronautical composites plates based on electromechanical impedance measurements and artificial neural networks. *Engineering Structures*. 2013;**56**:794-804.

[12] Na WS. Bolt loosening detection using impedance based non-destructive method and probabilistic neural network technique with minimal training data. *Engineering Structures*. 2021;**226**.

[13] Min J, Park S, Yun C-B, Lee C-G, Lee C. Impedance-based structural health monitoring incorporating neural network technique for identification of damage type and severity. *Engineering Structures*. 2012;**39**:210-20.

[14] Wang F. A novel autonomous strategy for multi-bolt looseness detection using smart glove and Siamese double-path CapsNet. *Structural Health Monitoring*. 2021.

[15] Du F, Wu S, Xing S, Xu C, Su Z. Temperature compensation to guided wave-based monitoring of bolt loosening using an attention-based multi-task network. *Structural Health Monitoring*. 2022:14759217221113443.

[16] Choy AW, editor Structural Health Monitoring with Deep learning. The International MultiConference of Engineers and Computer Scientists 2018 2018; Hong Kong.

[17] De Oliveira MA, Monteiro AV, Vieira Filho J. A New Structural Health Monitoring Strategy Based on PZT Sensors and Convolutional Neural Network. *Sensors*. 2018;**18**(9).

[18] Almeida JHL, Lopes LAR, Silva MAB, Amaral JLM, editors. Convolutional Neural Networks applied in the monitoring of metallic parts. International Joint Conference on Neural Networks; 2018 Jul 8, 2018 - Jul 13, 2018; Rio, Brazil: IEEE.

[19] de Rezende SWF, de Moura JdRV, Neto RMF, Gallo CA, Steffen V. Convolutional neural network and impedance-based SHM applied to damage detection. *Engineering Research Express*. 2020;**2**(3).

[20] Du F, Wu S, Xu C, Yang Z, Su Z. Electromechanical impedance temperature compensation and bolt loosening monitoring based on modified Unet and multitask learning. *Ieee Sens J*. 2021.

[21] Rai A, Mitra M. A transfer learning approach for damage diagnosis in composite laminated plate using Lamb waves. *Smart Materials and Structures*. 2022;**31**(6):065002.

[22] Wenbin Li CD, Pinzhuo Tian, Tiexin Qin, Xuesong Yang, Ziyi Wang, Jing Huo, Yinghuan Shi, Lei Wang, Yang Gao, Jiebo Luo. LibFewShot: A Comprehensive Library for Few-shot Learning. 2021.

[23] Oriol Vinyals CB, Timothy Lillicrap, Koray Kavukcuoglu, Daan Wierstra, editor Matching Networks for One Shot Learning. 30th Conference on Neural Information Processing Systems; 2016; Barcelona Spain: Curran Associates Inc., 57 Morehouse Lane, Red Hook, NY, United States.

[24] Finn C, Abbeel P, Levine S, editors. Model-agnostic meta-learning for fast adaptation of deep networks. International conference on machine learning; 2017: PMLR.

[25] Sung F, Yang Y, Zhang L, Xiang T, Torr PH, Hospedales TM, editors. Learning to compare: Relation network for few-shot learning. Proceedings of the IEEE conference on computer vision and pattern recognition; 2018.

[26] Jake Snell KS, Richard Zemel, editor Prototypical Networks for Few-shot Learning. 31st Conference on Neural

Information Processing Systems; 2017; Long Beach, CA, USA: Neural Information Processing Systems Foundation, Inc. (NeurIPS).
[27] Wu J, Zhao Z, Sun C, Yan R, Chen X. Few-shot transfer learning for intelligent fault diagnosis of machine. *Measurement*. 2020;**166**.
[28] Tao H, Cheng L, Qiu J, Stojanovic V. Few shot cross equipment fault diagnosis method based on parameter optimization and feature mertic. *Measurement Science and Technology*. 2022;**33**(11).
[29] Xu Y, Bao Y, Zhang Y, Li H. Attribute-based structural damage identification by few-shot meta learning with inter-class knowledge transfer. *Structural Health Monitoring*. 2020;**20**(4):1494-517.
[30] Giurgiutiu V, Zagrai AN. Embedded Self-Sensing Piezoelectric Active Sensors for On-Line Structural Identification. *Journal of Vibration and Acoustics*. 2002;**124**(1):116.
[31] Campeiro LM, da Silveira RZM, Baptista FG. Impedance-based damage detection under noise and vibration effects. *Structural Health Monitoring*. 2017;**17**(3):654-67.
[32] da Silveira RZM, Campeiro LM, Baptista FG. Performance of three transducer mounting methods in impedance-based structural health monitoring applications. *Journal of Intelligent Material Systems and Structures*. 2017;**28**(17):2349-62.
[33] Lim HJ, Kim MK, Sohn H, Park CY. Impedance based damage detection under varying temperature and loading conditions. *NDT & E International*. 2011;**44**(8):740-50.
[34] Wang Y, Yao Q, Kwok JT, Ni LM. Generalizing from a Few Examples. *ACM Computing Surveys*. 2021;**53**(3):1-34.
[35] Chen W-Y, Liu Y-C, Kira Z, Wang Y-CF, Huang J-B, editors. A Closer Look at Few-shot Classification. International Conference on Learning Representations; 2018.
[36] Jain P, Pachori RB. An iterative approach for decomposition of multi-component non-stationary signals based on eigenvalue decomposition of the Hankel matrix. *Journal of the Franklin Institute*. 2015;**352**(10):4017-44.
[37] Zhang Z, Li J, Du F, Xu C, editors. Design of Bolted Preload Electromechanical Impedance Monitoring Device for CubeSat. ASME International Mechanical Engineering Congress and Exposition; 2019: American Society of Mechanical Engineers.
[38] Kingma DP, Ba LJ. Adam: A Method for Stochastic Optimization. International Conference on Learning Representations; May 7-9, 2015; San Diego, USA2015.